International Journal of Computer Information Systems and Industrial Management Applications
ISSN 2150-7988 Volume 18(13s) 2026 pp. 1012-1025
https://doi.org/10.70917/ijcisim-2026-4145
Article

Low-PAPR Polarity-Split 4-LED MIMO-VLC Transmission with Direct-Channel 4D-ML Detection

Hiba K. Hussein[1], Saad M. Hardan[2,*]

[1,2]Department of Electrical Engineering, University of Tikrit, Tikrit, Iraq Corresponding Author:
Saad M. Hardan (E-mail : saad.m.hardan@tu.edu.iq)

Abstract: This paper presents a low-PAPR polarity-split four-LED MIMO-VLC transmission scheme for flat indoor optical channels. The proposed transmitter maps each complex QAM symbol into four nonnegative LED branches by separating the positive and negative polarities of the real and imaginary components. At the receiver, a direct-channel four-dimensional maximum-likelihood detector is used to estimate the transmitted QAM symbol directly from the photodetector-domain received vector. The proposed scheme is compared with GLIM-MAP, OSM-DCO-ML, and OSM-ACO-ML under fair spectral-efficiency settings with cyclic-prefix accounting. Simulation results over 4 x 4 flat MIMO-VLC channel matrices show that the proposed scheme provides a much lower PAPR than GLIM and OSM-ACO, and achieves clear BER gains over OSM-DCO under practical channels. At spectral efficiency = 4, the proposed scheme reduces the ML-search space by about 7.94 times relative to OSM-DCO, while avoiding the OFDM transmitter-side IFFT burden. The results indicate that the proposed scheme is a spectrally efficient and low-complexity flat-channel alternative for low-PAPR MIMO-VLC transmission.
Keywords: —Visible light communication, MIMO-VLC, polarity splitting, optical spatial modulation, GLIM, low PAPR, direct-channel 4D-ML detection, flat optical channel.

1. Introduction

Visible light communication (VLC) has attracted sustained interest as a complementary indoor wireless technology because light-emitting diode (LED) lighting infrastructure can support simultaneous illumination and data transmission [1]. Recent surveys highlight that MIMO-VLC can provide additional spatial degrees of freedom and improve data-rate scalability, but also introduces channel-correlation, receiver-design, and signal-format constraints that must be treated carefully [2, 3].

In practical intensity-modulation/direct-detection (IM/DD) links, the transmitted optical waveform must be real-valued and nonnegative [4, 5]. This requirement strongly influences the choice of modulation, waveform generation, biasing strategy, and receiver structure [6]. Recent work on optical wireless modulation and practical VLC front ends has emphasized that device bandwidth, optical power efficiency, receiver complexity, and modulation format should be considered jointly rather than optimizing one metric alone [7, 8].

Optical OFDM solutions, including DCO-OFDM and ACO-OFDM, are widely used because they provide flexible frequency-domain signal generation and can support high spectral efficiency [9]. However, they also require Hermitian-symmetric frame construction and IFFT/FFT processing, and they usually suffer from a high peak-to-average power ratio (PAPR)[10]. High PAPR is particularly undesirable in VLC systems because it increases the likelihood of LED nonlinear distortion, clipping, and dynamic-range inefficiency. These issues continue to motivate new signal processing and transceiver architectures for VLC systems [11].

MIMO-oriented OFDM schemes such as generalized LED index modulation (GLIM) and optical spatial modulation-assisted OFDM exploit the LED domain to satisfy optical unipolarity and improve spectral efficiency [12, 13]. GLIM is a strong BER-oriented benchmark because it combines OFDM signaling with MAP-based time-domain estimation[14]. Nevertheless, its OFDM waveform can exhibit a high PAPR. OSM-DCO and OSM-ACO provide alternative spatial-index baselines, but their required modulation order and ML search space grow rapidly when the target spectral efficiency increases[15]. For example, in a 4-LED system, OSM-ACO would require 16384-QAM to reach the high-spectral-efficiency case considered in this work [16].

Motivated by these observations, this paper investigates a low-PAPR polarity-split 4-LED MIMO-VLC transmission scheme over flat indoor optical MIMO channels. The proposed transmitter maps the real and imaginary parts of a QAM symbol into four nonnegative LED branches by separating positive and negative polarities. At the receiver, a direct-channel 4D-ML detector operates directly on the photodetector-domain received vector. The objective is not to claim universal BER superiority over GLIM; rather, the goal is to provide a spectrally efficient, low-PAPR, and lower-search-complexity flat-channel alternative that yields clear BER gains over OSM-DCO under practical, well-conditioned channel matrices.

The main contributions of this paper are summarized as follows:

1) A polarity-split 4-LED MIMO-VLC transmission structure is formulated for flat IM/DD optical MIMO channels, where four nonnegative LED branch signals represent each QAM symbol.

2) A direct-channel 4D-ML detector is developed to estimate the transmitted QAM symbol directly from the received photodetector-domain vector.

3) A fair spectral-efficiency comparison is established against GLIM-MAP, OSM-DCO-ML, and OSM-ACO-ML, including finite-block cyclic-prefix accounting.

4) The proposed scheme is evaluated in terms of BER, PAPR, robustness over multiple 4 x 4 VLC-MIMO channel matrices, and transceiver computational complexity, including real multiplication and addition/subtraction counts.

The remainder of this paper is organized as follows. Section 2 presents the proposed polarity-split 4-LED MIMO-VLC transmission system and the direct-channel 4D-ML detector. Section 3 describes the fair comparison setup with existing MIMO-OFDM benchmarks and provides the transceiver complexity analysis. Section 4 presents the simulation results and discussion. Section 5 concludes the paper.

2. Polarity-Split 4-LED MIMO-VLC Transmission with Direct-Channel 4D-ML Detection System

The overall architecture of the proposed flat-channel polarity-split 4-LED MIMO-VLC transceiver is shown in Fig. 1. The diagram summarizes the signal flow from input bits and QAM mapping to polarity splitting, optical scaling, propagation through the flat 4 x 4 MIMO-VLC channel, and direct-channel 4D-ML detection at the receiver.

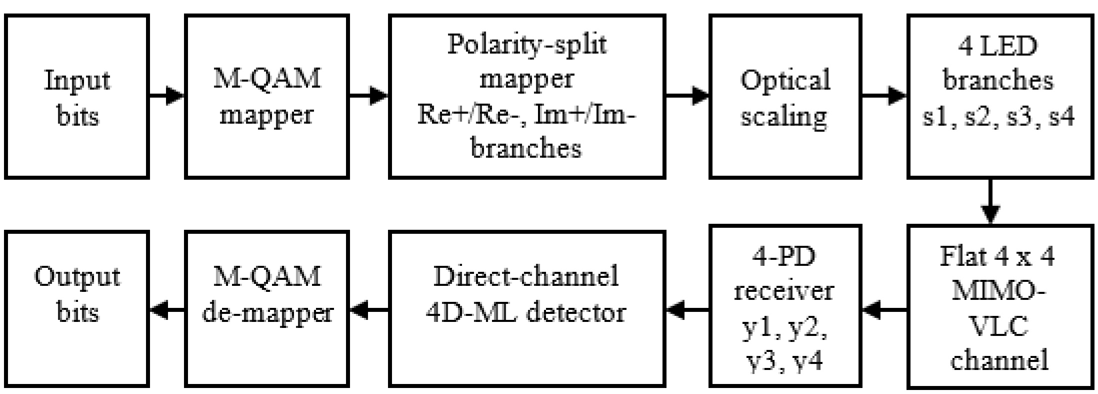

Fig. 1. Block diagram of the proposed flat-channel polarity-split 4-LED MIMO-VLC transceiver.

Let the information bit stream be mapped into a block of complex QAM symbols. The transmitted symbol is selected from the normalized M-QAM constellation X as

$$x[n] \in X, \quad n = 0,1, \dots, N-1. \tag{1}$$

Where N is the block length. The real and imaginary components are denoted by $a[n]$ and $b[n]$, respectively:

$$x[n] = a[n] + jb[n]. \tag{2}$$

For any real scalar u, its positive and negative components can be written in explicit max-form. In this paper, the LED mapping is written directly using this max-form. The four nonnegative LED branch signals are obtained from $a[n]$ and $b[n]$ as

$$s_1[n] = \max(a[n], 0), \quad s_2[n] = \max(-a[n], 0), \tag{3}$$

$$s_3[n] = \max(b[n], 0), \quad s_4[n] = \max(-b[n], 0). \tag{4}$$

The four-dimensional nonnegative transmit vector is therefore

$$\mathbf{s}[n] = [s_1[n], s_2[n], s_3[n], s_4[n]]^T. \tag{5}$$

An optical scaling coefficient α is applied to satisfy the target total optical mean power:

$$\mathbf{x}_{opt}[n] = \alpha\mathbf{s}[n]. \tag{6}$$

The coefficient alpha is chosen such that

$$E\{\mathbf{1}^T\mathbf{x}_{opt}[n]\} = P_{opt}, \tag{7}$$

where P_{opt} is the target total optical mean, and 1 is an all-one vector of length four. The received electrical signal vector at the four photodetectors is modeled as

$$\mathbf{y}[n] = \mathbf{H}\mathbf{x}_{opt}[n] + \mathbf{w}[n], \tag{8}$$

where H is the flat 4 x 4 optical MIMO channel matrix and $\mathbf{w}[n]$ is the additive electrical noise vector. The noise is modeled as zero-mean real Gaussian noise with covariance matrix:

$$\mathbf{R}_w = E\{\mathbf{w}[n]\mathbf{w}^T[n]\} = \sigma_w^2\mathbf{I}_4. \tag{9}$$

In (9), $E\{\cdot\}$ denotes the statistical expectation operator, $(\cdot)^T$ denotes the transpose operation, σ_w^2 is the electrical noise variance per photodetector, and I_4 is the 4 × 4 identity matrix.

For each candidate QAM symbol x_m, the corresponding real and imaginary parts are denoted by a_m and b_m. The candidate nonnegative vector is constructed as:

$$\mathbf{s}_m = [\max(a_m, 0), \max(-a_m, 0), \max(b_m, 0), \max(-b_m, 0)]^T. \tag{10}$$

After optical scaling, the noiseless received candidate is $\mathbf{H}\alpha\mathbf{s}_m$. The branch metric for candidate x_m is

$$d_m[n] = (\mathbf{y}[n] - \mathbf{H}\alpha\mathbf{s}_m)^T\mathbf{R}_w^{-1}(\mathbf{y}[n] - \mathbf{H}\alpha\mathbf{s}_m). \tag{11}$$

The proposed direct-channel 4D-ML decision rule is then

$$\hat{x}[n] = \arg\min_{x_m \in X} d_m[n]. \tag{12}$$

For spatially white noise, this is equivalent to the Euclidean-distance metric

$$\hat{x}[n] = \arg\min_{x_m \in X} \| \mathbf{y}[n] - \mathbf{H}\alpha\mathbf{s}_m \|_2^2. \tag{13}$$

Where R_w is the noise covariance matrix. The detected QAM symbol is then de-mapped using the same gray mapping as the transmitter.

3. Comparisons of 4D-ML and Existing MIMO-OFDM

3.1 Fair Spectral-Efficiency and Modulation-Order Setup

The target spectral efficiency is denoted by η in bits/s/Hz. For the proposed scheme and GLIM, the table-based spectral efficiency is

$$\eta_{prop} = \eta_{GLIM} = \log_2(M). \tag{14}$$

For OSM-DCO with n_T = 4 LEDs, the spectral efficiency is:

$$\eta_{OSM-DCO} = \frac{\log_2(Mn_T)}{2}. \tag{15}$$

For OSM-ACO, the corresponding spectral efficiency is

$$\eta_{OSM-ACO} = \frac{\log_2(Mn_T)}{4}. \tag{16}$$

With finite block length N and cyclic-prefix accounting N_{cp}, the proposed scheme and GLIM are reported using

$$\eta_{finite} = \frac{N}{N+N_{cp}} \log_2(M). \tag{17}$$

For OSM-DCO, where $K_{DCO} = \frac{N}{2} - 1$ positive-frequency subcarriers carry data, the finite-block spectral efficiency is

$$\eta_{OSM-DCO,finite} = \frac{K_{DCO}\log_2(Mn_T)}{N+N_{cp}}. \tag{18}$$

For OSM-ACO, where $K_{ACO} = \frac{N}{4}$ odd positive-frequency subcarriers are used, the corresponding finite-block spectral efficiency is

$$\eta_{OSM-ACO,finite} = \frac{K_{ACO}\log_2(Mn_T)}{N+N_{cp}}. \tag{19}$$

The modulation orders selected from these spectral-efficiency expressions are listed in Table I.

Table I. Modulation orders used for the fair spectral-efficiency comparison.

System	**At η = 2**	**At η = 4**
Proposed direct-channel 4D-ML	4-QAM	16-QAM
GLIM-MAP	4-QAM	16-QAM
OSM-DCO-ML	4-QAM	64-QAM
OSM-ACO-ML	64-QAM	excluded

At η = 4, OSM-ACO would require 16384-QAM for nT = 4. Therefore, it is excluded from the high-spectral-efficiency BER comparison because of its impractically high modulation order and excessive search complexity.

3.2 Transceiver Search-Space Complexity

The computational complexity of the considered systems is compared at the transceiver level, including both transmitter-side and receiver-side operations. The comparison is focused on the flat-channel case considered in this work. Therefore, no frequency-domain equalization or multipath processing is included for the proposed scheme.

The proposed transmitter is structurally simple. It performs QAM mapping, polarity splitting of the real and imaginary components, optical scaling, and direct transmission over four nonnegative LED branches. It does not require OFDM modulation, Hermitian-symmetric subcarrier construction, IFFT processing, subcarrier-index mapping, DC biasing, or clipping. In contrast, GLIM requires QAM mapping followed by an IFFT and time-domain separation into optical branches[17, 18]. OSM-DCO and OSM-ACO require spatial-index mapping, Hermitian-symmetric OFDM frame construction, IFFT processing, and additional optical-domain operations such as DC biasing for OSM-DCO or asymmetric clipping for OSM-ACO [19].

At the receiver, the proposed direct-channel 4D-ML detector searches over the original QAM constellation. Therefore, for each block, the number of candidate tests is

$$C_{\mathrm{prop}} = NM. \tag{20}$$

For $N = 256$ and $\eta = 4$, the proposed scheme uses $M = 16$, giving

$$C_{\mathrm{prop}} = 256 \times 16 = 4096 \tag{21}$$

candidate tests per block.

For OSM-DCO, ML detection is performed over the product of the QAM constellation and the active LED index. The number of data-bearing positive-frequency subcarriers is

$$K_{\mathrm{DCO}} = \frac{N}{2} - 1 = 127. \tag{22}$$

At $\eta = 4$, OSM-DCO requires $M = 64$ with $n_T = 4$, and hence the number of ML candidate tests is

$$C_{\mathrm{OSM-DCO}} = K_{\mathrm{DCO}} M n_T = 127 \times 64 \times 4 = 32512. \tag{23}$$

Thus, compared with OSM-DCO, the proposed detector reduces the ML search space by

$$\frac{C_{\mathrm{OSM-DCO}}}{C_{\mathrm{prop}}} = \frac{32512}{4096} \approx 7.94 \tag{24}$$

times at $\eta = 4$, while also avoiding the transmitter-side OFDM IFFT burden.

For OSM-ACO at $\eta = 4$, the required modulation order becomes $M = 16384$ for $n_T = 4$. Since the number of active odd positive-frequency subcarriers is $K_{\mathrm{ACO}} = N/4 = 64$, the corresponding number of candidate tests would be

$$C_{\mathrm{OSM-ACO}} = 64 \times 16384 \times 4 = 4194304. \tag{25}$$

This is approximately

$$\frac{C_{\mathrm{OSM-ACO}}}{C_{\mathrm{prop}}} = \frac{4194304}{4096} = 1024 \tag{26}$$

times larger than the proposed detector search space. This excessive search complexity, together with the impractically high modulation order, justifies excluding OSM-ACO from the $\eta = 4$ BER comparison.

The resulting transceiver-level search-space comparison at η = 4 is summarized in Table II.

Table II. Transceiver complexity comparison at η = 4.

System	**Transmitter processing**	**Receiver processing**	**Main search size at η = 4**
Proposed Direct-Channel 4D-ML	QAM mapping, polarity splitting, optical scaling; no OFDM IFFT	Direct-channel 4D-ML	$C_{\mathrm{prop}} = 4096$

System	Transmitter processing	Receiver processing	Main search size at η = 4
GLIM-MAP	QAM mapping, IFFT, separator	MAP estimation followed by FFT	MAP-based time-domain estimation
OSM-DCO-ML	Index mapping, Hermitian OFDM construction, IFFT, DC bias	FFT followed by ML over QAM and LED index	$C_{\mathrm{OSM-DCO}} = 32512$
OSM-ACO-ML	Index mapping, Hermitian OFDM construction, IFFT, asymmetric clipping	FFT followed by ML over QAM and LED index	$C_{\mathrm{OSM-ACO}} = 4194304$

Therefore, the proposed scheme offers a lower-complexity flat-channel transceiver than the OSM-based OFDM alternatives at high spectral efficiency. Although GLIM provides strong BER performance, it requires OFDM-domain processing and exhibits significantly higher PAPR. The proposed scheme therefore provides a favorable tradeoff among BER, PAPR, spectral efficiency, and computational complexity.

3.3 Detailed Real Multiplication and Addition/Subtraction Counts

To make the complexity comparison explicit, the number of real multiplications and real additions/subtractions is counted in addition to the ML-search size [20]. Additions and subtractions are counted together as real additions. Comparisons, memory transfers, index selection, and sign tests are not included. The channel-domain templates used by the ML and MAP metrics are assumed to be precomputed, since the channel is flat and remains fixed over the simulated block.

For a radix-2 length-N complex FFT or IFFT, the approximate real-operation counts are

$$\mathcal{M}_{\mathrm{FFT}}(N) = 2N\log_2 N, \tag{27}$$

$$\mathcal{A}_{\mathrm{FFT}}(N) = 3N\log_2 N, \tag{28}$$

where $\mathcal{M}(\cdot)$ and $\mathcal{A}(\cdot)$ denote the numbers of real multiplications and real additions/subtractions, respectively.

The proposed transmitter performs polarity splitting and optical scaling without OFDM modulation. If one real scaling multiplication is applied to each LED sample, the transmitter-side multiplication count is

$$\mathcal{M}_{\mathrm{TX}}^{\mathrm{prop}} = 4N, \tag{29}$$

and the corresponding transmitter-side addition count is approximately

$$\mathcal{A}_{\mathrm{TX}}^{\mathrm{prop}} \approx 0. \tag{30}$$

At the receiver, the proposed direct-channel 4D-ML metric for one candidate is

$$d_m = \|\mathbf{y}[n] - \boldsymbol{\mu}_m\|^2, \qquad \boldsymbol{\mu}_m = \mathbf{H}\mathbf{s}_m \tag{31}$$

For each candidate, the metric requires n_R real multiplications for squaring the residual elements and $2n_R - 1$ real additions/subtractions for residual formation and accumulation. Hence, for one block,

$$\mathcal{M}_{\mathrm{RX}}^{\mathrm{prop}} = NM_{\mathrm{prop}}n_R, \tag{32}$$

$$\mathcal{A}_{\mathrm{RX}}^{\mathrm{prop}} = NM_{\mathrm{prop}}(2n_R - 1). \tag{33}$$

Therefore, the total proposed transceiver count is

$$\mathcal{M}_{\mathrm{tot}}^{\mathrm{prop}} = 4N + NM_{\mathrm{prop}}n_R, \tag{34}$$

$$\mathcal{A}_{\mathrm{tot}}^{\mathrm{prop}} = NM_{\mathrm{prop}}(2n_R - 1). \tag{35}$$

GLIM requires one IFFT at the transmitter and one FFT at the receiver. Let C_{MAP} denote the effective number of conditional MAP hypotheses evaluated per time sample. The transmitter-side counts are approximated as

$$\mathcal{M}_{\mathrm{TX}}^{\mathrm{GLIM}} = 2N\log_2 N + 4N, \tag{36}$$

$$\mathcal{A}_{\mathrm{TX}}^{\mathrm{GLIM}} = 3N\log_2 N. \tag{37}$$

The receiver-side counts are

$$\mathcal{M}_{\mathrm{RX}}^{\mathrm{GLIM}} = 2N\log_2 N + NC_{\mathrm{MAP}}n_R, \tag{38}$$

$$\mathcal{A}_{\mathrm{RX}}^{\mathrm{GLIM}} = 3N\log_2 N + NC_{\mathrm{MAP}}(2n_R - 1). \tag{39}$$

Thus, the total GLIM transceiver counts are

$$\mathcal{M}_{\mathrm{tot}}^{\mathrm{GLIM}} = 4N\log_2 N + 4N + NC_{\mathrm{MAP}}n_R, \tag{40}$$

$$\mathcal{A}_{\mathrm{tot}}^{\mathrm{GLIM}} = 6N\log_2 N + NC_{\mathrm{MAP}}(2n_R - 1). \tag{41}$$

For OSM-DCO, the number of active positive-frequency data subcarriers is

$$K_{\mathrm{DCO}} = \frac{N}{2} - 1. \tag{42}$$

The transmitter requires n_T IFFT operations, optical scaling, and DC-bias addition. Therefore,

$$\mathcal{M}_{\mathrm{TX}}^{\mathrm{DCO}} = 2n_T N\log_2 N + n_T N, \tag{43}$$

$$\mathcal{A}_{\mathrm{TX}}^{\mathrm{DCO}} = 3n_T N\log_2 N + n_T N. \tag{44}$$

At the receiver, n_R FFT operations are required. The complex ML metric over n_R received branches requires $2n_R$ real multiplications and $4n_R - 1$ real additions/subtractions per candidate. Therefore,

$$\mathcal{M}_{\mathrm{RX}}^{\mathrm{DCO}} = 2n_R N\log_2 N + K_{\mathrm{DCO}}M_{\mathrm{DCO}}n_T(2n_R), \tag{45}$$

$$\mathcal{A}_{\mathrm{RX}}^{\mathrm{DCO}} = 3n_R N\log_2 N + K_{\mathrm{DCO}}M_{\mathrm{DCO}}n_T(4n_R - 1). \tag{46}$$

The total OSM-DCO counts are then

$$\mathcal{M}_{\mathrm{tot}}^{\mathrm{DCO}} = 2(n_T + n_R)N\log_2 N + n_T N + K_{\mathrm{DCO}}M_{\mathrm{DCO}}n_T(2n_R), \tag{47}$$

$$\mathcal{A}_{\mathrm{tot}}^{\mathrm{DCO}} = 3(n_T + n_R)N\log_2 N + n_T N + K_{\mathrm{DCO}}M_{\mathrm{DCO}}n_T(4n_R - 1). \tag{48}$$

For OSM-ACO, the number of active odd positive-frequency data subcarriers is

$$K_{\mathrm{ACO}} = \frac{N}{4}. \tag{49}$$

The transmitter requires n_T IFFT operations and optical scaling, while asymmetric clipping is treated as a comparison operation and is not counted as a real multiplication or addition. Hence,

$$\mathcal{M}_{\mathrm{TX}}^{\mathrm{ACO}} = 2n_T N\log_2 N + n_T N, \tag{50}$$

$$\mathcal{A}_{\mathrm{TX}}^{\mathrm{ACO}} = 3n_T N\log_2 N. \tag{51}$$

The receiver-side counts are

$$\mathcal{M}_{\mathrm{RX}}^{\mathrm{ACO}} = 2n_R N\log_2 N + K_{\mathrm{ACO}}M_{\mathrm{ACO}}n_T(2n_R), \tag{52}$$

$$\mathcal{A}_{\mathrm{RX}}^{\mathrm{ACO}} = 3n_R N\log_2 N + K_{\mathrm{ACO}}M_{\mathrm{ACO}}n_T(4n_R - 1). \tag{53}$$

Accordingly,

$$\mathcal{M}_{\mathrm{tot}}^{\mathrm{ACO}} = 2(n_T + n_R)N\log_2 N + n_T N + K_{\mathrm{ACO}}M_{\mathrm{ACO}}n_T(2n_R), \tag{54}$$

$$\mathcal{A}_{\mathrm{tot}}^{\mathrm{ACO}} = 3(n_T + n_R)N\log_2 N + K_{\mathrm{ACO}}M_{\mathrm{ACO}}n_T(4n_R - 1). \tag{55}$$

The relative ML-operation burden with respect to the proposed receiver is

$$\frac{\mathcal{M}_{\mathrm{ML}}^{\mathrm{DCO}}}{\mathcal{M}_{\mathrm{RX}}^{\mathrm{prop}}} = \frac{K_{\mathrm{DCO}}M_{\mathrm{DCO}}n_T(2n_R)}{NM_{\mathrm{prop}}n_R} = \frac{2K_{\mathrm{DCO}}M_{\mathrm{DCO}}n_T}{NM_{\mathrm{prop}}}, \tag{56}$$

$$\frac{\mathcal{A}_{\mathrm{ML}}^{\mathrm{DCO}}}{\mathcal{A}_{\mathrm{RX}}^{\mathrm{prop}}} = \frac{K_{\mathrm{DCO}} M_{\mathrm{DCO}} n_T (4n_R - 1)}{N M_{\mathrm{prop}} (2n_R - 1)}. \tag{57}$$

Similarly, for OSM-ACO,

$$\frac{\mathcal{M}_{\mathrm{ML}}^{\mathrm{ACO}}}{\mathcal{M}_{\mathrm{RX}}^{\mathrm{prop}}} = \frac{2K_{\mathrm{ACO}} M_{\mathrm{ACO}} n_T}{N M_{\mathrm{prop}}}, \tag{58}$$

$$\frac{\mathcal{A}_{\mathrm{ML}}^{\mathrm{ACO}}}{\mathcal{A}_{\mathrm{RX}}^{\mathrm{prop}}} = \frac{K_{\mathrm{ACO}} M_{\mathrm{ACO}} n_T (4n_R - 1)}{N M_{\mathrm{prop}} (2n_R - 1)}. \tag{59}$$

These equations show that the proposed flat-channel detector avoids the OFDM FFT/IFFT burden and keeps both the real-multiplication and real-addition counts proportional to NM_{prop}, whereas the OSM-based OFDM baselines scale with KMn_T in addition to the FFT/IFFT cost.

4. Simulation Results

This section evaluates the performance of the proposed polarity-split 4-LED MIMO-VLC scheme over flat 4×4 indoor optical MIMO channels. The proposed system is compared with GLIM-MAP, OSM-DCO-ML, and, at $\eta = 2$ only OSM-ACO-ML. The comparison is performed under equal target spectral-efficiency settings. A cyclic-prefix accounting factor is also reported for fairness, where $N = 256$ and $N_{\mathrm{cp}} = 64$. Therefore, the finite-block spectral efficiency of the proposed scheme and GLIM becomes $0.8\eta_{\mathrm{table}}$. For OSM-DCO, the finite-block spectral efficiency is slightly lower because only $N/2 - 1 = 127$ positive-frequency subcarriers are data-bearing.

For the main comparison, the $\mathbf{H}_{\mathrm{B}}^{a}$ channel is used because it represents a moderately conditioned flat MIMO-VLC channel. The $\mathbf{H}_{A}^{a}$ and $\mathbf{H}_{\mathrm{C}}^{p}$ channels are additionally used to verify robustness under severely ill-conditioned and better-conditioned channel conditions, respectively. The condition numbers of the three channel matrices are approximately 774.65, 13.24, and 3.45, respectively.

The flat 4 x 4 VLC-MIMO channel matrices used in the simulations are adopted from the physical-channel case study of Yesilkaya et al. [12], "Optical MIMO-OFDM With Generalized LED Index Modulation." These matrices are generated from the physical simulation-environment parameters reported in Table I of [12]. Therefore, Table I is cited as the source of the channel construction and is not reproduced here. The resulting channel matrices are written as follows:

$$\mathbf{H}_{\mathrm{A}}^{a} \approx 10^{-5} \times \begin{pmatrix} 0.3489 & 0.3288 & 0.3104 & 0.3288 \\ 0.3288 & 0.3489 & 0.3288 & 0.3104 \\ 0.3104 & 0.3288 & 0.3489 & 0.3288 \\ 0.3288 & 0.3104 & 0.3288 & 0.3489 \end{pmatrix} \tag{60}$$

$$\mathbf{H}_{\mathrm{B}}^{a} \approx 10^{-5} \times \begin{pmatrix} 0.4984 & 0.3005 & 0.2008 & 0.3005 \\ 0.3005 & 0.4984 & 0.3005 & 0.2008 \\ 0.2008 & 0.3005 & 0.4984 & 0.3005 \\ 0.3005 & 0.2008 & 0.3005 & 0.4984 \end{pmatrix} \tag{61}$$

$$\mathbf{H}_{\mathrm{C}}^{p} \approx 10^{-5} \times \begin{pmatrix} 0.5555 & 0.1866 & 0.1222 & 0.1866 \\ 0.1866 & 0.5555 & 0.1866 & 0.1222 \\ 0.1222 & 0.1866 & 0.5555 & 0.1866 \\ 0.1866 & 0.1222 & 0.1866 & 0.5555 \end{pmatrix} \tag{62}$$

In this work, $\mathbf{H}_{\mathrm{B}}^{a}$ is used as the main comparison channel, while $\mathbf{H}_{\mathrm{A}}^{a}$ and $\mathbf{H}_{\mathrm{C}}^{p}$ are used as the severely ill-conditioned stress-test and better-conditioned robustness cases, respectively.

Table III summarizes the modulation orders and finite-block spectral efficiencies used in the comparison. The column η_{table} follows the analytical expressions used to match the target spectral efficiency, while $\boldsymbol{\eta}_{\boldsymbol{finite},\mathbf{CP}}$ accounts for the finite block length and the CP overhead.

Table III. Spectral-efficiency setup with CP accounting.

Target η	System	M		,CP
2	Proposed Direct-Channel 4D-ML	4	2.000	1.600
2	GLIM-MAP	4	2.000	1.600
2	OSM-DCO-ML	4	2.000	1.5875
2	OSM-ACO-ML	64	2.000	1.600
4	Proposed Direct-Channel 4D-ML	16	4.000	3.200
4	GLIM-MAP	16	4.000	3.200
4	OSM-DCO-ML	64	4.000	3.175

At η = 2, the proposed scheme uses 4-QAM, GLIM also uses 4-QAM, OSM-DCO uses 4-QAM, and OSM-ACO requires 64-QAM. The BER behavior is shown in Fig. 2. GLIM provides the strongest BER performance at low target BER values, while OSM-ACO also performs competitively in BER at this spectral efficiency. However, the proposed scheme significantly outperforms OSM-DCO. At BER = 10^{-3}, the proposed scheme requires about 25.70 dB, whereas OSM-DCO requires about 31.64 dB, corresponding to an SNR gain of approximately 5.94 dB. The corresponding BER threshold values for the main $\mathbf{H}_B^a$ channel are summarized in Table IV.

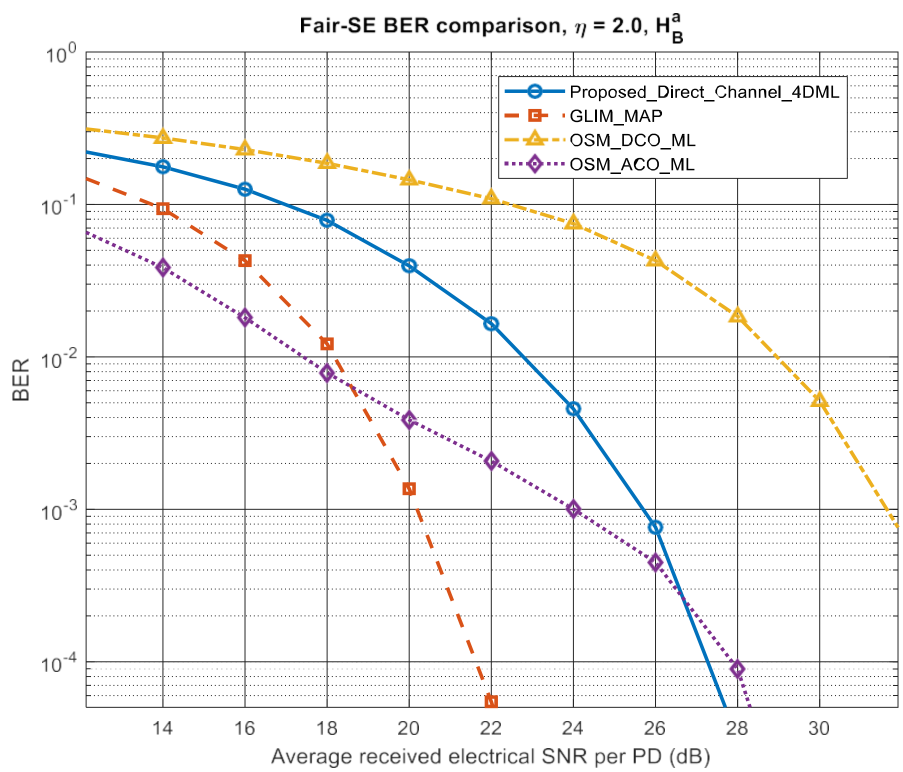

Fig. 2. BER comparison at target spectral efficiency η = 2 over the main channel. HBa

At η = 4, the proposed scheme and GLIM use 16-QAM, whereas OSM-DCO requires 64-QAM. OSM-ACO is not included at this spectral efficiency because it would require 16384-QAM for a 4-LED system, which is impractical and highly sensitive to noise. The corresponding BER curve is shown in Fig. 3. Under the $\mathbf{H}_B^a$ channel, the proposed scheme reaches BER = 10^{-3} at approximately 29.82 dB, while OSM-DCO requires approximately 39.97 dB. Thus, the proposed scheme provides an SNR gain of about 10.15 dB over OSM-DCO. At BER = 10^{-4}, the corresponding SNR values are approximately 32.23 dB and 43.61 dB, giving a gain of about 11.38 dB.

GLIM remains the strongest BER-oriented benchmark, requiring approximately 25.35 dB and 26.71 dB at BER = 10^{-3} and 10^{-4}, respectively, under the $\mathbf{H}_B^a$ channel. However, this BER advantage is obtained at the cost of OFDM-domain processing and significantly higher PAPR. The BER threshold values for both spectral-efficiency cases are reported in Table IV.

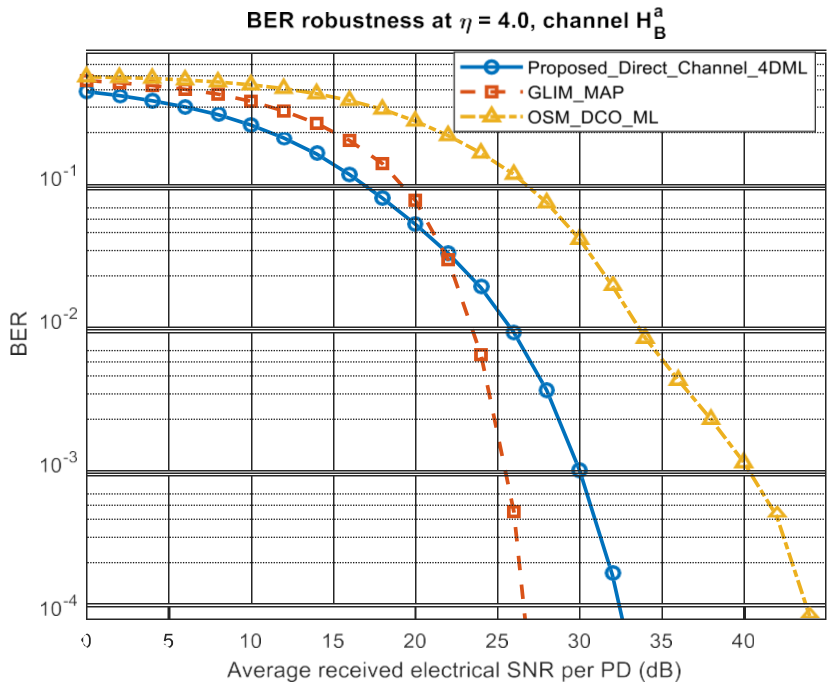

Fig. 3. BER comparison at target spectral efficiency η = 4 over the main channel. HBa

Table IV. BER threshold summary for the main channel. HBa

Target η	**System**	**M**	**SNR at BER 10^-3 (dB)**	**SNR at BER (dB)**
2	Proposed Direct-Channel 4D-ML	4	25.70	27.27
2	GLIM-MAP	4	20.19	21.62
2	OSM-DCO-ML	4	31.64	>32
2	OSM-ACO-ML	64	24.01	27.87
4	Proposed Direct-Channel 4D-ML	16	29.82	32.23
4	GLIM-MAP	16	25.35	26.71
4	OSM-DCO-ML	64	39.97	43.61

The PAPR results clarify the tradeoff between BER performance and optical waveform characteristics. At η = 2, the proposed waveform has nearly 0 dB PAPR, while GLIM and OSM-ACO exhibit PAPR values above 11 dB and 13 dB, respectively, at CCDF = . The η = 2 PAPR CCDF is shown in Fig. 4, and the corresponding numerical PAPR values are summarized in Table V. This confirms that the proposed scheme is particularly attractive when a low-PAPR optical waveform is required. 10-3

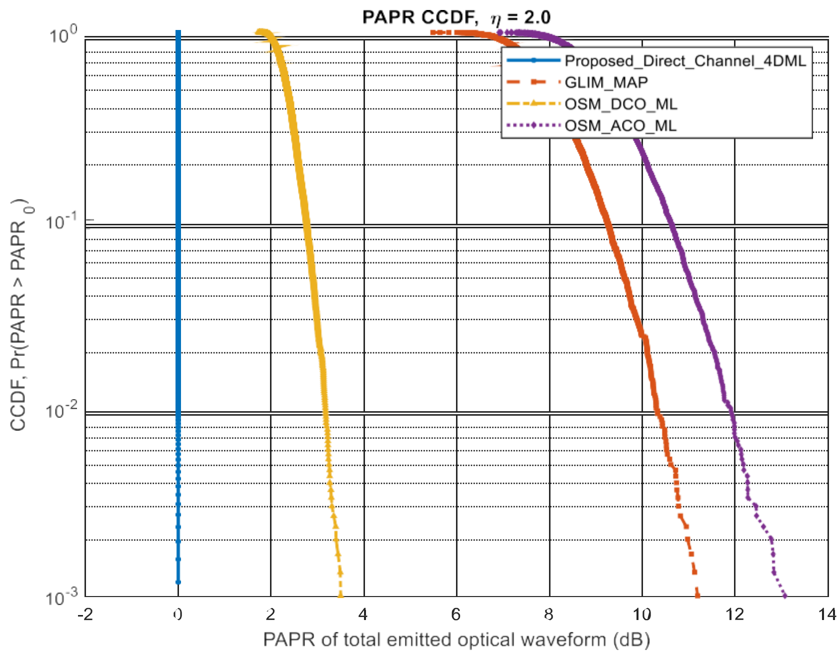

Fig. 4. PAPR CCDF comparison at target spectral efficiency η = 2.

At η = 4, the proposed scheme has a PAPR of about 3.67 dB at CCDF = 10^{-3}, whereas GLIM reaches approximately 11.91 dB. The corresponding PAPR CCDF is shown in Fig. 5, and the numerical metrics are included in Table V. Therefore, the proposed scheme reduces the PAPR by about 8.24 dB relative to GLIM. Compared with OSM-DCO, the proposed PAPR is very close, since the DC bias in OSM-DCO makes the total emitted optical waveform more stable when PAPR is computed after optical biasing.

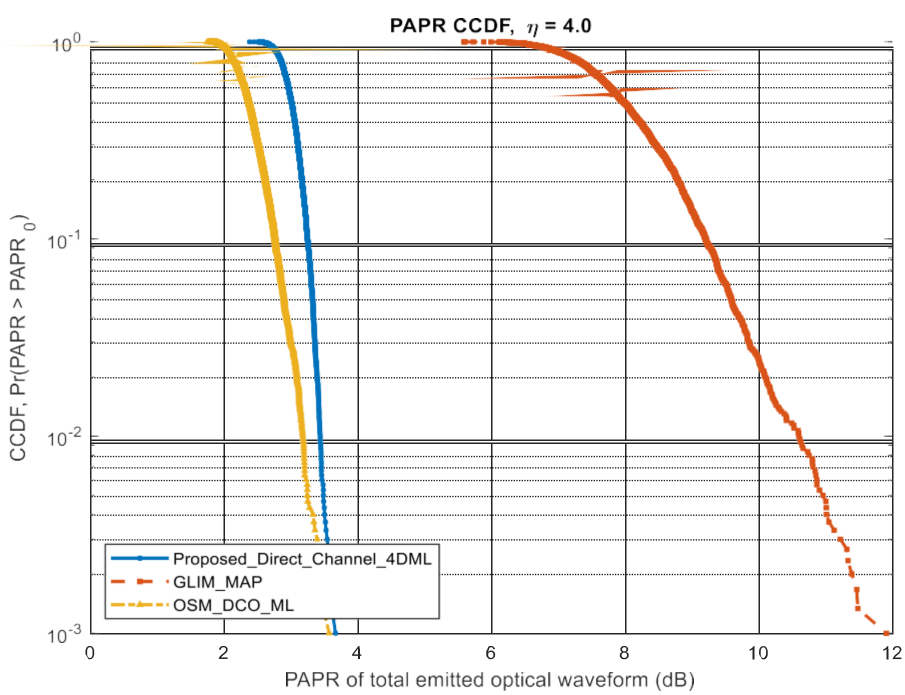

Fig. 5. PAPR CCDF comparison at target spectral efficiency η = 4.

Table V. PAPR summary.

Target η	System	Median PAPR (dB)	PAPR at CCDF (dB)
2	Proposed Direct-Channel 4D-ML	0.00	0.00
2	GLIM-MAP	8.01	11.20
2	OSM-DCO-ML	2.35	3.50
2	OSM-ACO-ML	9.27	13.08
4	Proposed Direct-Channel 4D-ML	3.01	3.67
4	GLIM-MAP	7.97	11.91
4	OSM-DCO-ML	2.37	3.58

The robustness results at η = 4 are summarized in Table VI and plotted in Fig. 6. They confirm that channel conditioning has a strong impact on all schemes. For the severely ill-conditioned $\mathbf{H}_A^a$ channel, GLIM and OSM-DCO achieve lower BER than the proposed scheme at low BER targets. This behavior is attributed to the very large condition number of $\mathbf{H}_A^a$, which strongly compresses the channel-domain distances of the proposed polarity-split constellation. Therefore, $\mathbf{H}_A^a$ is treated as a stress-test case rather than the main comparison channel.

For the better-conditioned $\mathbf{H}_C^p$ channel, Table VI shows that the proposed scheme reaches BER = 10^{-3} at about 21.56 dB, whereas OSM-DCO requires about 34.56 dB. This corresponds to an SNR gain of approximately 13.00 dB. At BER = 10^{-4}, the proposed scheme requires about 23.42 dB, while OSM-DCO requires about 37.45 dB, giving a gain of approximately 14.03 dB.

Table VI. Robustness summary at η = 4 over three flat 4 x 4 MIMO-VLC channels.

Channel	cond(H)	System	SNR at BER 10^{-3} (dB)	SNR at BER 10^{-4} (dB)
$\mathbf{H}_A^a$	774.65	Proposed Direct-Channel 4D-ML	64.80	67.45
$\mathbf{H}_A^a$	774.65	GLIM-MAP	52.65	54.49
$\mathbf{H}_A^a$	774.65	OSM-DCO-ML	58.39	62.02
$\mathbf{H}_B^a$	13.24	Proposed Direct-Channel 4D-ML	29.82	32.23
$\mathbf{H}_B^a$	13.24	GLIM-MAP	25.35	26.71
$\mathbf{H}_B^a$	13.24	OSM-DCO-ML	39.97	43.61
$\mathbf{H}_C^p$	3.45	Proposed Direct-Channel 4D-ML	21.56	23.42
$\mathbf{H}_C^p$	3.45	GLIM-MAP	18.76	20.32
$\mathbf{H}_C^p$	3.45	OSM-DCO-ML	34.56	37.45

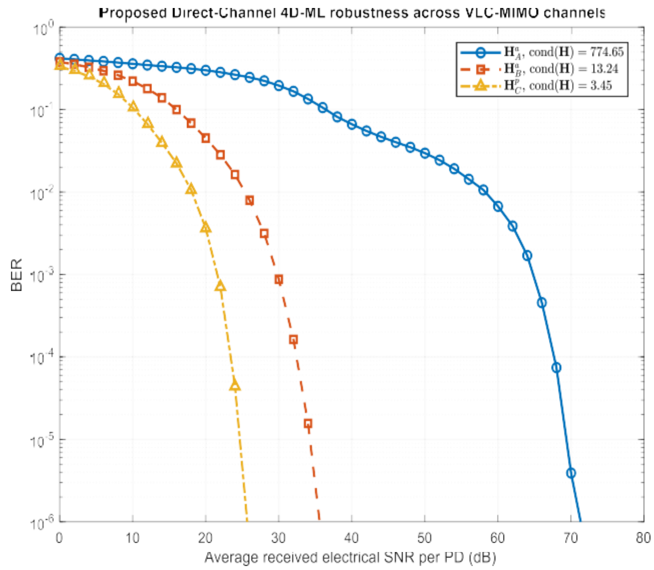

Fig. 6. Robustness of the proposed Direct-Channel 4D-ML detector over , , and at η = 4. HAaHBaHCp

Overall, the proposed scheme should not be interpreted as a BER-dominant alternative to GLIM. Instead, it provides a balanced flat-channel MIMO-VLC solution that combines low PAPR, high spectral efficiency, reduced ML search size, and strong BER gains over OSM-DCO in practical channel conditions.

For completeness, the severely ill-conditioned $\mathbf{H}_A^a$ channel is also plotted separately in Fig. 7. This curve is treated as a stress-test result because $\mathbf{H}_A^a$ has a very large condition number, and it is not used as the main performance-advantage case.

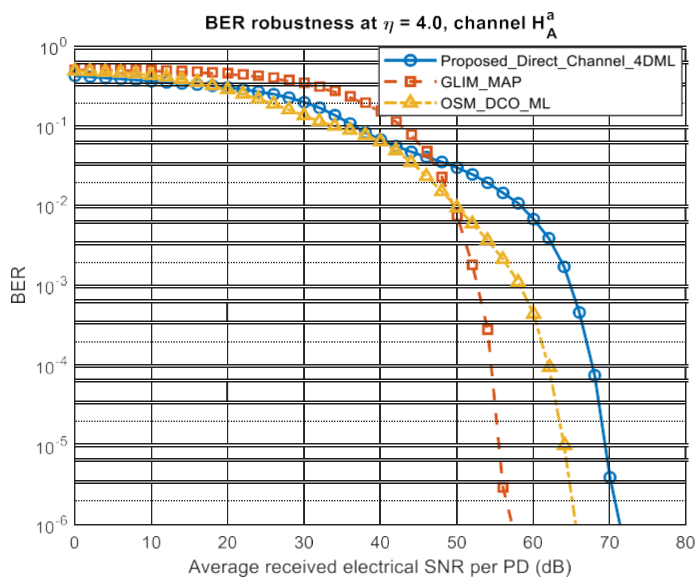

Fig. 7. BER robustness at η = 4 over the severely ill-conditioned channel. HAa

5. Conclusion

This paper investigated a low-PAPR polarity-split 4-LED MIMO-VLC transmission scheme for flat indoor optical MIMO channels. The proposed transmitter represents each QAM symbol by four nonnegative optical branches, while the receiver applies direct-channel 4D-ML detection in the photodetector domain. The study was intentionally restricted to flat 4 x 4 MIMO-VLC channels to isolate the effect of the proposed polarity-split signaling and detector structure without introducing multipath equalization or SC-FDE processing. Under fair spectral-efficiency settings, the proposed scheme demonstrated a strong PAPR advantage over GLIM and OSM-ACO. At η = 4, it also provided substantial BER gains over OSM-DCO for the practical and HC channel matrices. The severely ill-conditioned channel was included as a stress-test case and showed that channel conditioning strongly affects all schemes; in that case, GLIM and OSM-DCO achieved lower BER than the proposed method at low target BER levels. Therefore, the proposed scheme is not claimed to be universally superior to GLIM in BER. Rather, it offers a balanced flat-channel MIMO-VLC solution that combines low PAPR, high spectral efficiency, reduced ML search complexity relative to OSM-DCO at high η, and favorable BER performance under practical, well-conditioned channel matrices. Future work may extend the proposed architecture to frequency-selective multipath MIMO-VLC channels and SC-FDE-based receiver structures. HBaHAa

References

1. W. Popoola, T. Z. Gutema, and M. Elamassie, "Visible light communication (VLC) basics," in Handbook of Radio and Optical Networks Convergence: Springer, 2024, pp. 1-35.
2. M. A. S. Sejan, M. H. Rahman, M. A. Aziz, D.-S. Kim, Y.-H. You, and H.-K. Song, "A comprehensive survey on MIMO visible light communication: Current research, machine learning and future trends," Sensors, vol. 23, no. 2, p. 739, 2023.
3. O. Narmanlioglu and M. Uysal, "Multi-user massive MIMO visible light communications with limited pilot transmission," IEEE Transactions on Wireless Communications, vol. 21, no. 6, pp. 4197-4211, 2021.
4. H. Ou, K. Zhu, C. Ye, and Y. Hu, "An intensity-modulation direct-detection radio-over-fiber link with a tunable transfer function," Optics Communications, vol. 284, no. 8, pp. 2126-2130, 2011.
5. S. D. Dissanayake and J. Armstrong, "Comparison of aco-ofdm, dco-ofdm and ado-ofdm in im/dd systems," Journal of lightwave technology, vol. 31, no. 7, pp. 1063-1072, 2013.
6. N. Kikuchi and R. Hirai, "Intensity-modulated / direct-detection (IM/DD) Nyquist pulse-amplitude modulation (PAM) signaling for 100-Gbit/s/λ optical short-reach transmission," in 2014 The European Conference on Optical Communication (ECOC), 21-25 Sept. 2014 2014, pp. 1-3, doi: 10.1109/ECOC.2014.6964069.
7. H. Chun et al., "Optimum device and modulation scheme selection for optical wireless communications," Journal of Lightwave Technology, vol. 39, no. 8, pp. 2281-2287, 2021.
8. R. Kısacık et al., "A 130 nm CMOS receiver for visible light communication," Journal of Lightwave Technology, vol. 40, no. 12, pp. 3681-3687, 2022.
9. X. Zhang, Z. Babar, P. Petropoulos, H. Haas, and L. Hanzo, "The evolution of optical OFDM," IEEE communications surveys & tutorials, vol. 23, no. 3, pp. 1430-1457, 2021.
10. I. K. Sileh, A. A. Abdulkaf, M. K. Hussein, and S. M. Hardan, "Complex Signal Mapping for Improving Spectral Efficiency of Li-Fi Systems," Journal of Telecommunications and Information Technology, no. 3, pp. 58-62, 2019.
11. Z. Geng, F. N. Khan, X. Guan, and Y. Dong, "Advances in visible light communication technologies and applications," in Photonics, 2022, vol. 9, no. 12: MDPI, p. 893.
12. A. Yesilkaya, E. Basar, F. Miramirkhani, E. Panayirci, M. Uysal, and H. Haas, "Optical MIMO-OFDM with generalized LED index modulation," IEEE Transactions on Communications, vol. 65, no. 8, pp. 3429-3441, 2017.
13. S. M. Hardan, A. A. Abdulkafi, S. H. Thalij, and S. S. Jumaah, "Mobility aware of WDM-based CMO OFDM communication system," Journal of Optical Communications, vol. 44, no. s1, pp. s1739-s1745, 2024.
14. M. Le Tran, S. Kim, T. Ketseoglou, and E. Ayanoglu, "LED selection and MAP detection for generalized LED index modulation," IEEE Photonics Technology Letters, vol. 30, no. 19, pp. 1695-1698, 2018.
15. S. M. Hameed, S. M. Abdulsatar, and A. A. Sabri, "Performance enhancement for visible light communication based ADO-OFDM," Optical and Quantum Electronics, vol. 53, no. 6, p. 339, 2021.
16. S. Ma et al., "Spectral and energy efficiency of ACO-OFDM in visible light communication systems," IEEE transactions on wireless communications, vol. 21, no. 4, pp. 2147-2161, 2021.
17. C. Chen, "Special issue on “visible light communication (VLC)”," in Photonics, 2022, vol. 9, no. 5: MDPI, p. 284.
18. R. Le Priol, "Improvements of VLC (Visible Light Communication) transmissions under illumination constraints: theoretical studies and experiments," INSA de Rennes, 2022.
19. Y. Li, D. Tsonev, and H. Haas, "Non-DC-biased OFDM with optical spatial modulation," in 2013 IEEE 24th annual international symposium on personal, indoor, and mobile radio communications (PIMRC), 2013: IEEE, pp. 486-490.
20. I. S. Sergeev, "On the real complexity of a complex DFT," Problems of Information Transmission, vol. 53, no. 3, pp. 284-293, 2017.